Chemical Engineering Science 131 (2015) 197–212

Contents lists available at ScienceDirect

Chemical Engineering Science

journal homepage: www.elsevier.com/locate/ces

Comparisons of intra-tablet coating variability using DEM simulations, asymptotic limit models, and experiments

Ben Freireich [a], Rahul Kumar [b], William Ketterhagen [c], Ke Su [d], Carl Wassgren [b,e,*], J. Axel Zeitler [d]

[a] Core Research and Development, The Dow Chemical Company, Midland, MI 48667, USA
[b] School of Mechanical Engineering, Purdue University, West Lafayette, IN 47907-2088, USA
[c] Worldwide Research and Development, Pfizer, Inc., Groton, CT 06340, USA
[d] Department of Chemical Engineering and Biotechnology, University of Cambridge, Pembroke Street, Cambridge CB2 3RA, UK
[e] Department of Industrial and Physical Pharmacy (by courtesy), Purdue University, West Lafayette, IN 47907-2091, USA

HIGHLIGHTS

- DEM simulations exhibit asymptotic intra-tablet coating thickness behavior.
- Representative tablet model with shadowing predicts asymptotic coating thickness.
- Asymptotic intra-tablet coating thickness correlates with tablet sphericity.
- Smallest coating thickness on smallest radii of curvature portions of tablet band.
- Coating thickness predictions compare well to experimental measurements.

ARTICLE INFO

Article history:
Received 27 December 2014
Received in revised form
11 March 2015
Accepted 15 March 2015
Available online 26 March 2015

Keywords:
Coating variability
Pharmaceuticals
DEM
Tablet shape
Tablet coating

ABSTRACT

Discrete element method (DEM) computer simulations are used to investigate intra-tablet coating thickness variability. Two new post-processing algorithms are presented. The first algorithm uses an image-based method to track the exposure to a simulated spray of small area panels on each tablet's surface so that the distribution of spray exposure times over the tablet's surface can be determined directly from DEM data. The second algorithm predicts the asymptotic limit of intra-tablet coating uniformity. This second algorithm includes the influence of tablet orientation and shadowing when considering exposure to the spray, averaged over many tablets.

The DEM simulations produce the first direct evidence that non-spherical tablets approach asymptotic intra-tablet coating variability values. The asymptotic limits are predicted well using the new asymptotic prediction model. In general, tablet caps have thicker coatings than tablet bands. Moreover, tablets that have a more elongated shape tend to have less coating on the smaller radius of curvature portions of the bands. Of particular importance in this new asymptotic modeling approach is the inclusion of shadowing effects. When shadowing is not included and only tablet orientation is considered, the predictions over-predict the asymptotic intra-tablet coating variability values and also change the observed rank order of the asymptotic values for different tablet shapes. The asymptotic intra-tablet coating variability values using the new algorithm correlate reasonably well with tablet sphericity, with increasing sphericity improving coating uniformity.

This paper also presents the first attempt to directly compare experimental and simulated coating thickness distributions. The asymptotic coating thickness predictions compare well qualitatively with terahertz thickness measurements made on tablets from coating experiments. Unfortunately, only qualitative comparisons could be made due to the limited number of tablets sampled experimentally and differences in spray zone areas and flux distributions. The tablets in the experiments, however, displayed similar features as those found in the simulations.

* Corresponding author at: School of Mechanical Engineering, Purdue University, West Lafayette, IN 47907-2088, USA. Tel.: +1 765 494 5656.
E-mail address: wassgren@purdue.edu (C. Wassgren).

http://dx.doi.org/10.1016/j.ces.2015.03.013

1. Introduction

Coating pharmaceutical tablets is an important process in the manufacture of drug products. Tablets are coated for a wide variety of reasons (Turton, 2008), such as controlling the bioavailability and release profile of the drug (referred to as a functional coating), masking the color, taste, or odor of the drug, ensuring product identification and esthetics, and providing protection to the tablet cores.

The objective of a coating process is to apply a thin film of polymer onto a tablet's surface. Traditionally, the coating is applied in a batch process in which a fixed number of tablets are tumbled inside a rotating, perforated drum with baffles to mix the tablets while spraying a coating solution at the surface of the bed. Tablets are coated as they pass through the spray zone. Heated air flowing through the tablet bed evaporates the solvent causing the polymeric chains in the coating to intermingle and lock to form a film on the surface of each tablet. Fig. 1 shows a schematic of a typical batch tablet coating process.

The coating process is terminated when the tablets achieve a target average weight gain. At the end of the coating process, the quality of the coating is examined for defects such as peeling, picking and sticking, bridging, chipping, twinning, roughness, and color variability (Tousey, 2005). Especially for functional coatings, the variability in the coating mass, i.e., the mass gained during the coating process, is also an important criterion for determining the effectiveness of the coating process. There are two types of coating variability: the variability in coating mass between different tablets, referred to as inter-tablet coating variability, and the variability in the coating mass over the surface of a single tablet, which is referred to as intra-tablet coating variability. In the present work, the intra-tablet coating variability is of particular interest.

2. Background

The variation in coating mass over a single tablet's surface can be quantified using the variation in the film thickness over the tablet's surface. This variability is referred to as the intra-tablet coating variability and is defined as the ratio of the standard deviation of the film thickness, σ_h, to the mean film thickness over the tablet's surface, μ_h,

$$CoV_{\text{intra}} = \frac{\sigma_h}{\mu_h}, \tag{1}$$

where the subscript h refers to the film thickness over a differential area.

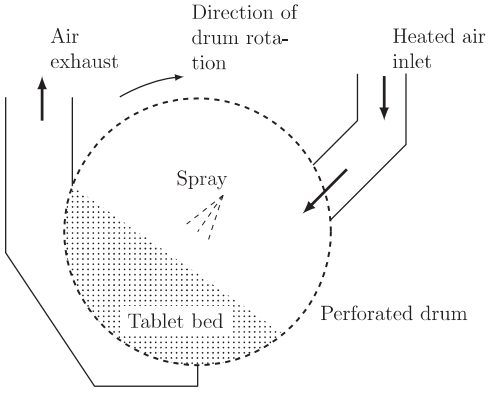

Fig. 1. Schematic of a batch tablet coating process in a perforated drum.

Much of the previous work investigating intra-tablet coating variability relied upon experiments to correlate tablet shape and operating parameters with CoV_{intra}. The coating variability was measured in these experiments using a variety of methods including micrometers and microscopy (Pérez-Ramos et al., 2005), near infrared imaging (Pérez-Ramos et al., 2005), laser induced breakdown spectroscopy (Madamba et al., 2007), and terahertz pulse imaging (Ho et al., 2007; Brock et al., 2013). Video-based experiments in which tablet caps were painted black while the bands remained white have also been used (Pérez-Ramos, 2006), with the duration of exposed pixels acting as a surrogate for coating. In all of these investigations, the caps of the tablets were found to have thicker coatings, or appear preferentially in the video frames, as compared to the tablet bands.

Pan speed and pan fill level have been observed to have a minor, but measurable influence on the degree of intra-tablet coating variability. Increasing the rotational speed of the pan generally reduces the coating variability as observed in both experiments (Wilson and Crossman, 1997) and discrete element method (DEM) computer simulations (Ketterhagen, 2011; Freireich et al., 2011). The video experiments of Pérez-Ramos (2006) showed inconsistent trends with pan speed, but the effect was minor regardless. The experiments by Brock et al. (2013) showed little dependence on drum speed. Increasing the fill level decreased the anticipated CoV_{intra} in Pérez-Ramos's experiments, but caused an increase in the computations of Ketterhagen and experiments of Brock et al. Tablets that are more agitated and thus presenting a wider range of orientations while passing through the spray zone are expected to have smaller coating variability. Indeed, Alexander et al. (2002) and Pandey et al. (2006) showed that larger pan speeds and fill levels result in larger surface speeds and thus an increased degree of agitation would be expected. Ketterhagen did note that at his smallest fill level, which was much smaller than what was used in the other researchers' experiments, the bed flow was more violent than at the larger fill levels.

Previous work has shown that the most significant parameter affecting intra-tablet coating variability is tablet shape. Specifically, tablet shapes with a larger probability of having a particular orientation when passing through the spray zone are expected to have larger CoV_{intra} values. For example, Wilson and Crossman (1997) coated four tablet shapes with the variability increasing for round, oval, capsule, and large oval tablets, respectively. Ketterhagen (2011) found similar results in his DEM simulations, with more spherical and smaller aspect ratio tablets correlating with smaller orientation indexes (which imply reduced variability). Suzzi et al. (2012) also used DEM simulations to examine coating variability for biconvex, oval, and spherical tablet shapes. They found that spherical tablets resulted in the largest angular velocities on the free surface and, thus, presumably the smallest intra-tablet coating variability, consistent with the previously described studies.

Freireich and Wassgren (2010) demonstrated mathematically that a tablet having any preferred orientation, which is most likely to occur for non-spherical tablets, will approach an asymptotic CoV_{intra} value at large coating times, with a greater degree of preferred orientation resulting in larger asymptotic coating variability. Furthermore, the time to approach this asymptotic value decreases with increasing preferred orientation. In contrast, the CoV_{intra} for a spherical tablet, which has no preferred orientation, will decrease inversely with the square root of time and will not reach an asymptotic value. The fact that an asymptotic value is reached for intra-tablet coating variability is significant since this behavior is significantly different than the behavior observed for *inter*-tablet coating variability. If the mixing is poor in a coating pan, it may appear that the CoV_{inter} approaches an asymptote, but as long as there is at least some mixing, the CoV_{inter} will eventually

be proportional to the inverse square root of time after a sufficiently long period of time (Kumar et al., 2014).

Freireich et al. (2011) confirmed the existence of an asymptotic CoV_{intra} for almond, bullet, half moon, shield, and standard round concave tablet shapes using a combined DEM–Monte Carlo modeling approach. Spherical tablets followed the predicted inverse square root trend. Since the DEM simulations were time consuming, computations for the full duration of a coating process were not performed. Instead, the DEM simulations were used to generate a frequency distribution of spray zone tablet orientations. The Monte Carlo algorithm randomly sampled a tablet orientation from this distribution, "coated" the tablet, and then repeated the process for a large number of coating trials. The coating process consisted of dividing the surface of the tablet into a collection of small-area panels. For a given orientation, the panels exposed to the spray were assumed to accumulate an amount of coating proportional to the projected area of the panel. The influence of the neighboring tablets was not considered.

Freireich et al. (2011) also attempted to correlate the asymptotic CoV_{intra} values with the tablets' sphericities, aspect ratios, and band-to-total surface area, but did not find satisfactory trends. Additionally, the authors found that tilting the angle of the simulated spray in the spanwise direction reduced the coating variability significantly since the tablet bands were coated more frequently. This finding has yet to be tested experimentally.

The current work investigates intra-tablet coating uniformity for several tablet shapes using a combination of DEM simulations, multi-scale modeling, and experiments. The differences between previous efforts and the current one are that: (1) the current DEM simulations are performed for a sufficiently long time to approach the asymptotic intra-tablet coating behavior, (2) a new multi-scale modeling approach is proposed that includes the shadowing effects of neighboring tablets, and (3) the model predictions are compared qualitatively to experimental measurements of coating thickness distributions using terahertz imaging.

3. Discrete element method (DEM) simulations

The DEM simulations in the current work are an extension of the previously reported study by Ketterhagen (2011). As with this previous study, the movement of various tablet shapes in a lab-scale coating pan are modeled, but in the present work, new tablet shapes are modeled and, most significantly, the simulations are run for a longer period of time, out to 1800 s, to approximately match the duration of the experimental coating batches.

A CAD drawing of the lab-scale LDCS 5 (Vector, Marion, IA) film coater used in the experiments, shown in Fig. 2, was created and imported into the commercial DEM software EDEM® (DEM Solutions, Edinburgh, Scotland). The pan dimensions, rotation speed, and baffle configuration were all matched as closely as possible to the experimental conditions, some of which are summarized in Table 1. Batches of four different tablet shapes, shown in Table 2, were simulated. The batch size for each shape was 1 kg.

Following Ketterhagen (2011), the EDEM default contact model Hertz–Mindlin (no-slip) was used in this work, with the material properties and interaction parameters summarized in Table 1. The material properties of the tablets and coating pan were selected to represent placebo tablets and the stainless steel pan, respectively, with the exception of the shear moduli, which have been reduced to decrease the computational time required for the simulations. The interaction parameter values, adopted from the earlier Ketterhagen (2011) work, have been shown to successfully simulate the tablet flow in an experimental system as determined using a machine vision system with a tracer tablet. Further, most of the parameter values coincide with experimental measurements made for a variety of tablets (Bharadwaj et al., 2010; Hancock et al., 2010; Just et al., 2013). However, there is variability in the reported experimental data. For instance, Hancock et al. (2010) reported tablet–tablet friction coefficients near 0.0 while Just et al. (2013) reported a range

Table 1
Parameters used in the DEM simulations.

Parameter	Value
Pan rotational speed	22 RPM
Pan loading	1 kg
Number of baffles	4
Number of tablets	~770
Tablet mass	1300 mg
Contact force models	Hertz–Mindlin (default)
Tablet shear modulus	1×10^6 Pa
Tablet Poisson's ratio	0.25
Tablet density	1500 kg/m^3
Steel shear modulus	3×10^6 Pa
Steel Poisson's ratio	0.3
Steel density	7500 kg/m^3
Coeff. of static friction (sphere–sphere)	0.5
Coeff. of static friction (sphere–cylinder)	0.5
Coeff. of rolling friction (sphere–sphere)	0.0
Coeff. of rolling friction (sphere–cylinder)	0.0
Coeff. of restitution (sphere–sphere)	0.5
Coeff. of restitution (sphere–cylinder)	0.5
Total simulation time	1800 s
Time between output data samples	0.02 s

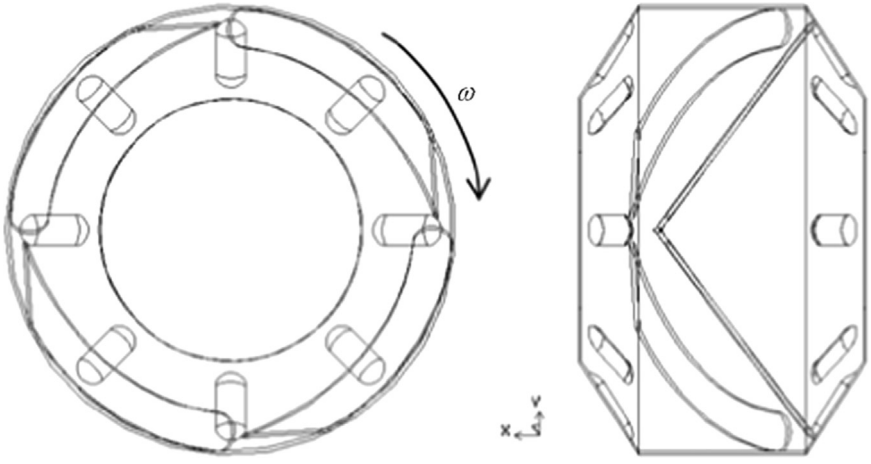

Fig. 2. Schematic of the LDCS 5 1.3L film-coating pan.

Table 2
Images, including photographs (top) and glued-sphere representations (bottom) #in EDEM, of each of the four tablet shapes studied.

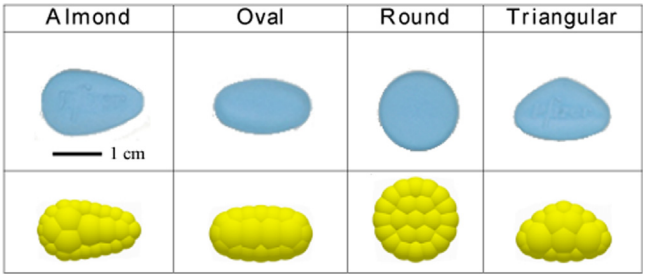

of values greater than 0.4. There are similar discrepancies for tablet–steel friction coefficients as Hancock et al. (2010) reported values between 0.1 and 0.7 while Just et al. (2013) reported measured values only near 0.1.

The sensitivity to the interaction parameter values has not been assessed here. Freireich et al. (2009) found that the bulk kinematic behavior of spheres in a rotating drum were insensitive to contact stiffness and coefficient of restitution over a wide range of values. Other researchers have reported sensitivity to the friction coefficients used in DEM simulations, however. Kalbag et al. (2008) described an increase in the tablet appearance frequency in the spray zone with increasing friction coefficient (both tablet–tablet and tablet–steel were identical). That work had focused on inter-tablet coating variability, and so it is unclear what the effect, if any, is for tablet orientation in the spray zone, and thus, intra-tablet coating variability. Others, such as Yamane et al. (1998) and Pandey et al. (2006) have observed an increase in the dynamic angle of repose with increasing friction coefficients, with the greatest sensitivity present for smaller friction coefficients. Just et al. (2013) also observed sensitivity in the angle of repose to the tablet–steel friction coefficient. Despite measuring values near 0.1, they artificially increased the friction coefficient in the DEM simulations to a value greater than 0.45 in order to attain a dynamic angle of repose in the simulations that was similar to that from experiments. Thus, while there is some sensitivity to the friction coefficient values, there is reasonable confidence that the values used here are suitable for simulating the coating process, especially since good agreement with experimental results has been obtained previously (Ketterhagen, 2011).

The spray is not directly modeled within the DEM simulation. Rather, the position and orientation of each tablet are exported every 0.02 s for additional analysis as described in detail in the following section. Further assumptions in the model include neglecting the effects of drying air, transfer of coating between tablets before drying, and possible variation in the material properties and interaction parameters as tablets receive coating.

4. Coating algorithm

The image-based algorithm described by Kumar et al. (2014) was modified to track the surfaces of tablets exposed to the "spray" in the DEM simulations. As with previous DEM studies, tablets were not actually sprayed in the simulation, but instead the duration of their exposed surfaces in a designated spray zone was tracked. By tracking the duration that panels were exposed to the spray, the intra-tablet coating variability for each tablet and the entire batch could be calculated.

In order to determine what parts of a tablet's surface were exposed to the "spray" (in the simulations, a specific region on the surface of the tablet bed is used instead of modeling the spray droplets), the surface of the tablet was divided into N_p triangular panels. The same panels were used on each of the tablets of the same shape. In order to uniquely identify a panel j on a tablet i, a unique ID number, p_{id}, was assigned to the panel as follows:

$$p_{id} = iN_p + j, \tag{2}$$

where i varied from 0 to N, the total number of tablets in the system, while j went from 0 to N_p. Fig. 3 shows the panels used for the different tablet shapes. The panels were made using the ANSYS ICEM CFD surface mesher (ANSYS, 2014) starting from the CAD file for each of the tablet shapes.

In order to calculate the coating accumulated by the panels, the panels were assigned an RGB color based on their ID

$$R = \left\lfloor \frac{p_{id}}{256^2} \right\rfloor, G = \left\lfloor \frac{p_{id}}{256} \right\rfloor, B = p_{id}\%256, \text{and} (R,G,B) \neq (255,255,255), \tag{3}$$

where "$\lfloor \ldots \rfloor$" is the floor operator and "%" is the modulo operator. A value of (R, G, B)=(255, 255, 255) was reserved for the background white color. Eq. (3) ensured that a unique color was assigned to each panel. Since each of the RGB components could have an integer value ranging from 0 to 255, up to $256^3 - 1$ ($\sim$16.5 million) panels could be uniquely identified using the given algorithm. Fig. 4 shows a typical rendering of the panels using OpenGL where the tablets are viewed from the spray frame of reference. Note that these colors differ by one integer value in terms of the RGB color and are difficult to distinguish visually.

After the panels were rendered, the spray region was identified as shown in Fig. 4. A rectangular spray zone was used in the present work for simplicity, although any other shape, for example a circular or elliptical shape, could be used as well. The spray was oriented normal to the bed surface and had spanwise and streamwise dimensions of 76.2 mm by 38.1 mm, respectively. These dimensions were chosen to closely match those of the experiments. Once the spray region on the bed was prescribed, the visible pixel colors in this region were obtained using the OpenGL library command glReadPixels. The coating volume on the panels was determined using

$$V_{ij} = \sum_{n=1}^{T} (k_V c_{ij,n}), \tag{4}$$

where V_{ij} is the total coating volume for panel j on tablet i, k_V is a proportionality constant to convert from pixels to a coating volume, $c_{ij,n}$ is the number of pixels from panel j on tablet i in the spray region at the nth time step, and T is the total number of time steps in the simulation. The proportionality constant k_V was calculated by setting the mean coating thickness measured from DEM at the end of the simulation equal to the experimentally measured coating thickness at the end of the coating process.

At any given time-step there was a distribution of coating volume over all of the panels. Note that panels had different areas and thus the coating volume accumulated on a panel depended on its area. In order to exclude the effect of the varying area of the panels, the volume accumulated by the panels was divided by the panel area to give the coating thickness on the panel, h_{ij}

$$h_{ij} = \frac{V_{ij}}{A_j}, \tag{5}$$

where A_j is the panel area. For a given tablet i, the mean, μ_i and standard deviation, σ_i, of the coating thickness over the panels was

$$\mu_i = \frac{1}{N_p} \sum_{j=1}^{N_p} h_{ij} A_j, \tag{6}$$

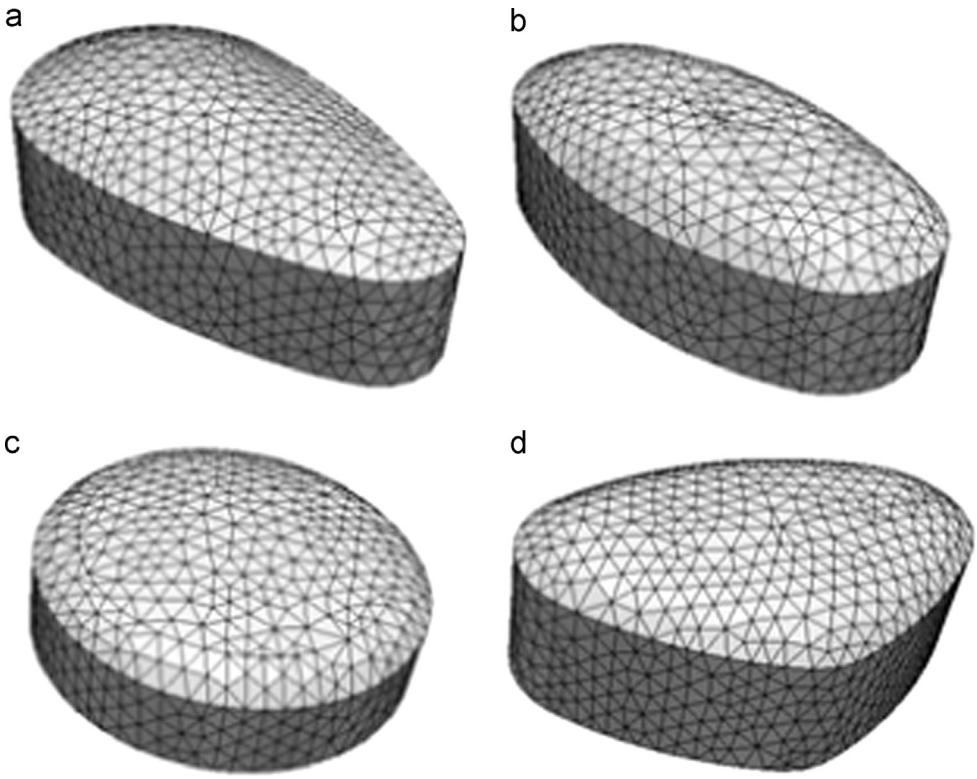

Fig. 3. Panels used for the various tablet shapes. (a) Almond tablet with 1856 panels; (b) oval tablet with 1704 panels; (c) round tablets with 1702 panels; and (d) triangular tablets with 1848 panels.

$$\sigma_i^2 = \frac{1}{N_p}\sum_{j=1}^{N_p}(h_{ij}-\mu_i)^2 A_j. \tag{7}$$

The intra-tablet coating variability for the tablet i, $CoV_{\text{intra},i}$, was defined as the ratio of σ_i to μ_i. Following Freireich and Wassgren (2010), the batch intra-tablet coating variability was defined as the ratio of the square root of the average of σ_i^2 to the average of μ_i over all the tablets

$$CoV_{\text{intra}} = \frac{\sqrt{\frac{1}{N}\sum_{i=1}^{N}\sigma_i^2}}{\frac{1}{N}\sum_{i=1}^{N}\mu_i}. \tag{8}$$

Note that taking the average of each tablet's CoV_{intra} gives a similar result as Eq. (8) after a sufficiently long period of time (see Appendix).

5. Representative tablet method for predicting the asymptotic CoV_{intra}

As with previous DEM-only studies of tablet coating, the computational time required to model an entire coating process is generally impractical. Hence, a combined modeling approach is used here in which short duration DEM simulations are used to inform a separate model to predict long term coating behavior, similar to the DEM–Monte Carlo model initially proposed by Freireich et al. (2011). This section describes the current model, termed the "representative tablet method" and compares it to the Freireich et al. (2011) model.

Freireich et al. (2011) developed a combined DEM–Monte Carlo algorithm to obtain the asymptotic value of the intra-tablet coating variability using tablet orientation distributions derived from short DEM simulations. For each tablet located in the spray region during each time step of the DEM simulation, determined using a CPU-based ray tracing method, the tablet's orientation was recorded in order to produce a distribution of tablet orientations. Note that the simulation time required to achieve a stationary distribution of orientations (less than ~80 s) was much shorter than the time expected to reach the asymptotic CoV_{intra} directly in the DEM simulations (more than one hour). The Monte Carlo portion of the model proceeded by randomly sampling an orientation from the distribution, "coating" the exposed surface of a single tablet with the given orientation relative to the spray, calculating the CoV_{intra}, then repeating the process. Similar to the method outlined previously, the tablet's surface was discretized into small areas, or panels, so that the coating could be spatially resolved over the surface. The amount of coating applied to a panel was proportional to the projected area of that panel exposed to the spray. The primary disadvantage of this approach was that the partial occlusion of tablets, which occurs in an actual coating process, was not accounted for in the algorithm.

In the new approach, tablets are coated in a post-processing step using the data generated by the DEM simulations and the coating algorithm described in Section 4. At any given time step, the tablets in the spray zone are identified and the distribution of coating mass on the panels of those tablets is obtained. Each tablet that is coated is considered a single coating trial of a representative tablet. Essentially, the coating corresponding to a particular panel on every tablet over all times is accumulated on a single representative tablet. Note that the effects of tablet orientation and neighboring tablet occlusion are automatically accounted for in this approach since the OpenGL coating algorithm is used. In addition, the total amount of coating on the tablet does not factor into the CoV_{inta} calculation since it is the relative distribution of coating that is important. A flowchart detailing the new algorithm is shown in Fig. 5. As with the Freireich et al. DEM–Monte Carlo model, this new method utilizes data from short duration DEM simulations, but the new approach is faster than the previous model since the new approach relies on a different CoV_{intra} averaging

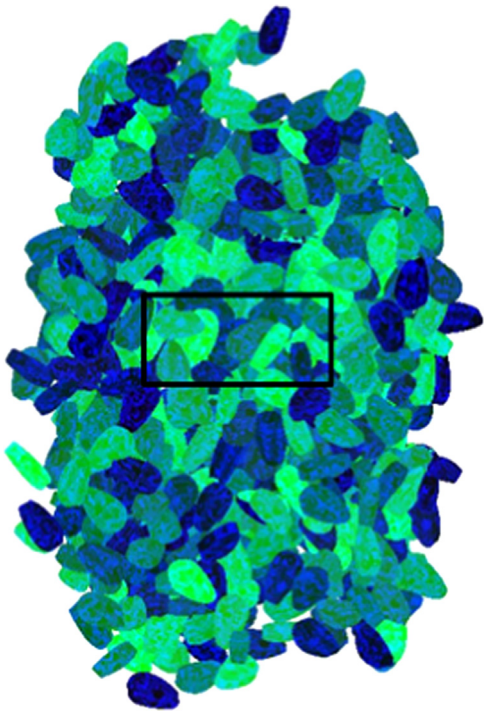

Fig. 4. OpenGL rendering of the panels on each of the tablets (shown here for almond tablets) as seen from the spray frame of reference. The spray zone is identified by the rectangular region.

scheme (refer to Appendix) and the OpenGL algorithm is parallelized in hardware rather than relying on CPU-based ray-tracing. In addition, the new approach automatically accounts for tablet occlusion, which was not considered in the previous approach. Table 3 summarizes the three algorithms considered in the present work.

6. Coating experiments

Coating experiments were performed in order to provide comparisons to the models described in the previous sections. In these experiments, placebo tablets were manufactured from a blend consisting of a 2:1 mixture of microcrystalline cellulose (Avicel PH101) and lactose (Lactose 316 Fast Flo), 3% sodium starch glycolate, and 1% magnesium stearate. Tablets of four different shapes: almond, oval, round, and triangular (refer to Table 2), were manufactured on a Kilian T-100 tablet press with each shape having a mean tablet mass of 1300 mg. The tooling used in the experiments produced debossment features on the almond and triangular tablet shapes, which are not included in the DEM simulations. The dimensions of each tablet are summarized in Table 4 along with various shape measures.

The tablets were coated with a 20% w/w suspension of Blue Opadry II (Colorcon, Harleysville, PA) in a lab-scale LDCS 5 film coater (Vector, Marion, IA) with a 1.3 L pan rotating at 22 RPM. The pan has four custom manufactured baffles that span the width of the pan and are positioned in an alternating orientation (Fig. 2). Tablet batches of 1 kg were coated until a mean weight gain of 4% was obtained using a spray nozzle aligned perpendicular to the tablet bed with a nozzle-to-bed distance of approximately 5 cm. The spray zone is elliptical in shape with dimensions of approximately 3.81 cm by 7.62 cm in the streamwise and spanwise directions, respectively. The spray rate was held constant at 7.5 g/min. Following completion of the film coating, tablets were randomly chosen from each batch for analysis via terahertz (THz) imaging. Table 5 lists the number of tablets that were sampled for each of the tablet shapes.

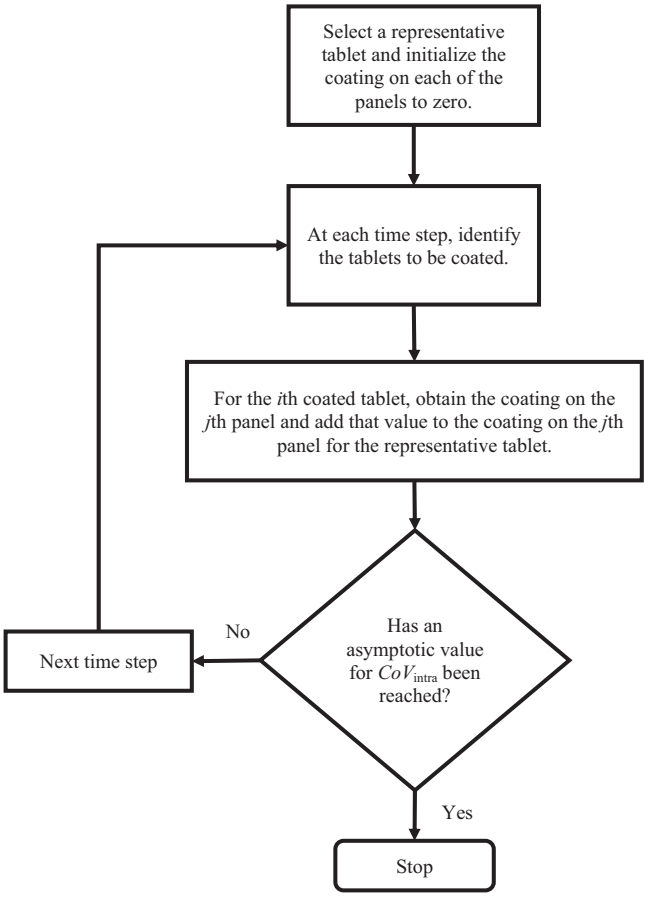

Fig. 5. A flowchart showing the new representative tablet approach used to predict the asymptotic CoV_{intra} value.

7. Terahertz (THz) imaging measurements

The coated tablets were analyzed using a terahertz pulsed imaging TPI Imaga 2000 coating scan system (Teraview Ltd., Cambridge, UK) as previously described in Zeitler et al. (2007). Terahertz reflection time-domain waveforms were acquired over approximately 120 min per tablet in the point-to-point mode at a step size of 200 μm over the entire surface of the tablets, yielding between 16,000 and 18,000 individual coating thickness measurements per tablet (depending on geometry). The lateral spatial resolution over the surface of each tablet is limited by diffraction to 200 μm, while the axial (depth) resolution is governed by the pulse duration and sampling resolution in the time-domain (Shen and Taday, 2008). The refractive index of the coating material was estimated to be 1.53, based on the surface reflectivity of the tablets and using x-ray microtomography (Skyscan 1172, Bruker, Kontich, Belgium) (Russe et al., 2012). The uncertainty in thickness was estimated using terahertz pulsed imaging to be better than 2% based on the refractive index and previous validation (Russe et al., 2012). Coating thickness analysis was performed using TPIView (version 3.0.3, TeraView Ltd.) and the 3D coordinates and corresponding coating thickness and surface reflectivity values were processed using MATLAB (R2013a, MathWorks, Natick MA, USA). All data points close to the edges of the tablet's center band and in the debossing of the tablet were removed by thresholding against the surface reflectivity, which is the most sensitive measure of the scattering losses. The threshold was set to 12% reflectivity compared to the reference reflection from a silver coated mirror with all pixels exceeding the threshold being included in the subsequent analysis and pixels falling below this value being

Table 3
Summary of the algorithms used in the present work.

Model name	DEM-only	Monte Carlo – orientation only	Representative Tablet
Source	Present work	Freireich et al. (2011)	Present work
Approach	OpenGL-based analysis of DEM position and orientation data	MC analysis of DEM orientation data	OpenGL-based analysis of DEM position and orientation data
Input data	DEM sim. (1800 s)	DEM sim. (~100 s)	DEM sim. (~100 s)
Orientation effects	Yes	Yes	Yes
Shadowing effects	Yes	No	Yes
Computational time	Long	Moderate	Moderate
Prediction(s)	CoV_{inter} and CoV_{intra} at any time in the simulation	asymptotic CoV_{intra}	asymptotic CoV_{intra}

Table 4
Summary of the dimensions, sphericity, aspect ratio, and band-to-face surface area for each of the tablet shapes. These quantities are based on the tablets' CAD file representations.

Tablet shape	Length, L (or diameter, D) [mm]	Width, W [mm]	Thickness, T [mm]	Surface area, A [mm^2]	Volume, V [mm^3]	Sphericity, $S=(36\pi V^2)^{1/3}/A$	Aspect ratio, $AR=(L+W)/(2T)$	Band-to-face surface area ratio, A_B/A_F
Almond	20.6	12.1	7.86	644.7	1182	0.8383	2.201	0.6385
Oval	19.2	10.8	7.86	588.6	1112	0.8816	1.829	0.6317
Round	15.9	n/a	6.64	584.5	1042	0.8502	2.556	0.3842
Triangular	19.2	12.5	8.46	652.1	1300.	0.8835	1.886	0.1561

Table 5
Number of tablets sampled for analysis using THz imaging for different tablet shapes.

Tablet shape	Number of tablets sampled
Almond	10
Oval	2
Round	3
Triangular	1

considered reflections originating from sites affected strongly by scattering.

8. Results

In the following subsections, results from the DEM simulations, the multiscale model described in Section 5, and the experiments are presented.

8.1. Direct prediction of CoV_{intra} using DEM-only

Fig. 6a plots the DEM predictions of the CoV_{intra} as a function of time for the four tablet shapes. The CoV_{intra} values near the beginning of the simulation are almost identical. Although it is off to the left of the plot in Fig. 6a, all of the tablet shapes started ($t\rightarrow 0$) at a CoV_{intra} of approximately 10. The CoV_{intra} values decrease with time then appear to approach an asymptotic limit as predicted by Freireich and Wassgren (2010), although the simulations do not reach this limit for any of the shapes in the 1800 s of simulation time. At the end of the 1800 s, the oval tablet has the smallest CoV_{intra}, followed by the triangular tablet, the round tablet, and finally the almond tablet. As noted in Freireich and Wassgren, the larger CoV_{intra} values, e.g., the almond shape, appear to approach an asymptotic limit more rapidly than the smaller values, e.g., the oval. The experiments by Brock et al. (2013) reported that longer run times resulted in smaller intra-tablet coefficients of variation, consistent with the current findings. Indeed, in their studies using a design of experiments approach, the duration of the coating experiment had the most significant impact of all the variables they examined. The experiments of Pérez-Ramos et al. (2005) in which the band and face coating thicknesses were measured as a function of time for round tablets (Fig. 5 of their paper) reach an asymptotic limit, although the large amount of experimental scatter in their work (particularly at times less than 40 min) makes the uncertainty in determining the time to reach this asymptotic limit too large for meaningful comparisons with the work presented here.

The inter-tablet coating coefficient of variation, CoV_{inter} corresponding to Fig. 6a is plotted in Fig. 6b. In all cases, after approximately 10 s the CoV_{inter} follows the expected inverse square root of time trend as predicted (see, for example, Kumar et al., 2014). The CoV_{inter} curves are nearly identical for all tablet shapes. A comparison of Fig. 6a and b emphasizes the point that unlike inter-tablet coating variability, coating for a longer period of time does not always result in a smaller intra-tablet coating variability, particularly after a sufficiently long period of time.

Fig. 7 plots the average predicted coating thickness distributions at the end of the simulations for each of the tablet shapes. This average was calculated over the ~770 tablets in each simulation. The color scale in the figures denotes the coating thickness in microns. In the simulations, the thickness is actually given in terms of pixels exposed per unit area, but a scaling factor k_V, which is described in Sections 4 and 8.3, is used to convert to microns in an attempt to match the spray flux used in the experiments.

It is clear that the shape of the tablet has a significant impact on the intra-tablet coating variability. In all instances, the tablet caps have a larger coating thickness than the bands, consistent with previous studies. The oval tablet, due to its long shape, can roll about its long axis, exposing the sides more frequently compared to the other tablet shapes. The relatively smaller coating mass at the front and back of the tablet is also consistent with this idea that the ease with which the tablet can roll affects the coating distribution. Thus, the oval tablet has the best intra-tablet coating uniformity. It is also not surprising that the triangular shape, which is only slightly different from the oval shape, has a smaller intra-tablet coating variability compared to the round and almond tablets. The round tablet is more pancake shaped and thus cannot roll as easily and, as a result, the band of the tablet gets relatively less coating. It is interesting to note that for round tablets, the coating thickness at the center of the cap is less than the thickness near the edge. This difference is due to shadowing of tablets by neighboring tablets and is discussed in more detail in the

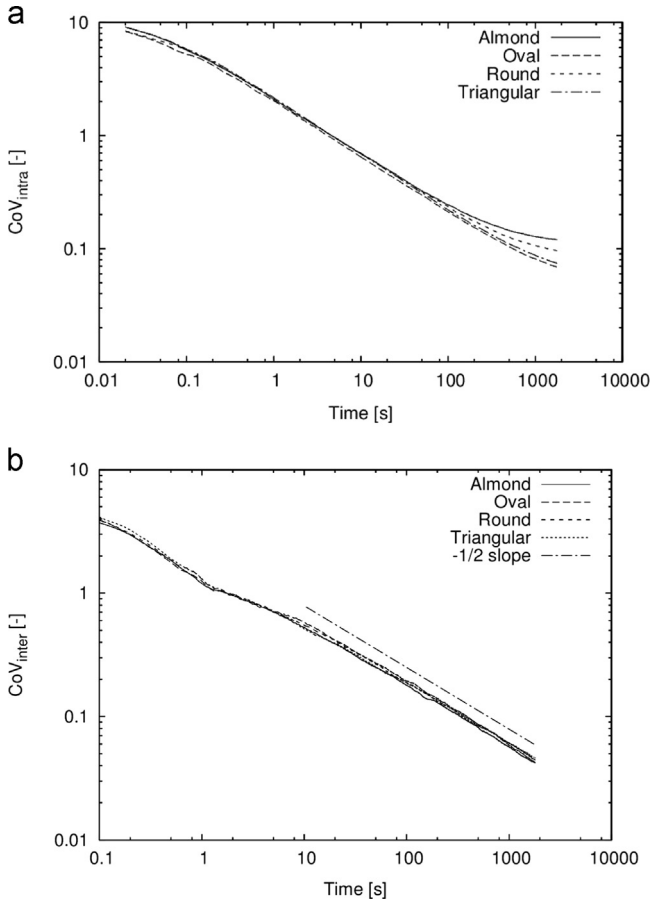

Fig. 6. (a) DEM predictions of intra-tablet coefficient of variation, CoV_{intra}, plotted as a function of time for the four tablet shapes examined in this study. (b) The corresponding inter-tablet coefficient of variation, CoV_{inter}, plotted as a function of time for the same tablets.

following section. A similar result was observed in the experiments of Möltgen et al. (2012) and Madamba et al. (2007). However, the experiments of Brock et al. (2013) and Russe et al. (2012) showed little variation in coating thickness over the cap surface. The different observations may be the result of using tablets with different shapes (discussed in Section 8.2).

The simulations also show a wide variation in the coating thicknesses on the tablet bands. Round tablets are the exception, with virtually no variation with angular position and minor variation with vertical position. The other tablet shapes in Fig. 7 show significant band thickness variations with both angular position and height. In particular, smaller radii of curvature portions of the band, such as the ends of the oval and triangular tablets, have smaller coating thicknesses as compared to larger radii of curvature portions. This behavior may be related to the fact that tablets are more likely to roll about axes passing through the smaller radii of curvature, thus exposing the larger radii of curvature bands more frequently.

It is important to note that individual tablets can have coating distributions significantly different than the averages shown in Fig. 7. Fig. 8 plots the coating distributions on four randomly chosen almond tablets, with each tablet having approximately the same coating mass. The same basic features observed for the average coating thickness appear in the individual tablets, such as larger coating thicknesses on the cap as opposed to the band and the smallest coating thickness occurring on the band at the wide and narrow ends of the tablet. The widely varying thickness distributions, however, indicate that although the mean coating thickness distribution may be satisfactory, individual tablets may not be. Indeed, the experiments of Brock et al. (2013) show a wide range of individual tablet face-to-band coating thickness ratios. Furthermore, in order to meaningfully compare experimental measurements to DEM predictions, a sufficiently large number of samples must be collected and measured in the experiments.

Fig. 9 plots the standard deviation over all individual tablet CoV_{intra} values as a function of time for the round tablets (i.e., the standard deviation of $CoV_{intra,i}$ as defined in Eq. (11) in the Appendix). Note that the data begin only after all tablets have some coating on them so that the individual tablet CoV_{intra} values are well defined. Although not plotted here, the distribution of individual tablet CoV_{intra} values are normally distributed after a sufficiently long period of time. The standard deviation closely follows a power law trend with the power exponent equaling approximately -0.57 for the given data. Thus, although coating for a longer period of time will not necessarily improve a tablet's CoV_{intra} due to the existence of an asymptote, it will improve the consistency in CoV_{intra} values between tablets.

8.2. Predictions of asymptotic CoV_{intra}

Although the DEM-only simulations were not able to reach the asymptotic CoV_{intra} values in the 1800 s of simulation time, these asymptotic values can be estimated using the Monte Carlo method of Freireich et al. (2011) and the new representative tablet modeling approach described in Section 5. Fig. 10 plots the predictions from these two models superimposed over the data from Fig. 6. The new modeling approach is more accurate than the model originally proposed by Freireich et al., which over-predicts the asymptotic CoV_{intra} in all cases. The new modeling approach gives an asymptotic value smaller than the DEM simulations, as should be the case because the asymptote has not been reached. The relative rankings of the tablet shapes also changes between the two asymptotic models. The representative tablet model gives a ranking consistent with the DEM simulations after 1800 s: oval, triangular, round, and almond shapes in order from smallest to largest asymptotic CoV_{intra}. The Freireich et al. model switches the order of the round and almond shapes. The fundamental difference between the two asymptotic modeling approaches is that the new approach includes the effects of shadowing by neighboring particles, which apparently has a significant impact on the intra-tablet coating variability. In addition to being more accurate, the new modeling approach is conceptually simpler insomuch that distributions of quaternions do not need to be collected or sampled for the new approach.

Prior studies have attempted to correlate CoV_{intra} with tablet shape measures (Ketterhagen, 2011; Freireich et al., 2011) with limited success. We attempt a similar correlation here, but using the asymptotic values predicted from the representative tablet model. Three shape measures are considered: aspect ratio, $AR=(L+W)/(2T)$, sphericity, $S=(36\pi V^2)^{1/3}/A$, and the band-to-face surface area ratio, A_B/A_F, where V and A are the tablet volume and surface area, L, W, and T are the tablet length, width, and thickness, and A_B and A_F are the tablet band and face surface areas. The values for these shape measures are based on the tablets' CAD file representations and are provided for the four tablet shapes in Table 4. The asymptotic CoV_{intra} values are plotted as a function of these measures in Fig. 11. The best correlation is with the tablet sphericity; however, the correlation is not perfect. The fact that a larger sphericity generally results in a smaller asymptotic CoV_{intra} is consistent with previous work (Wilson and Crossman, 1997; Ketterhagen, 2011; Freireich et al., 2011).

Maps of the predicted asymptotic coating thicknesses using the new approach and the approach of Freireich et al. (2011) are shown in Fig. 12. The maps using the new asymptotic coating model are quite similar to the maps generated at the conclusion of

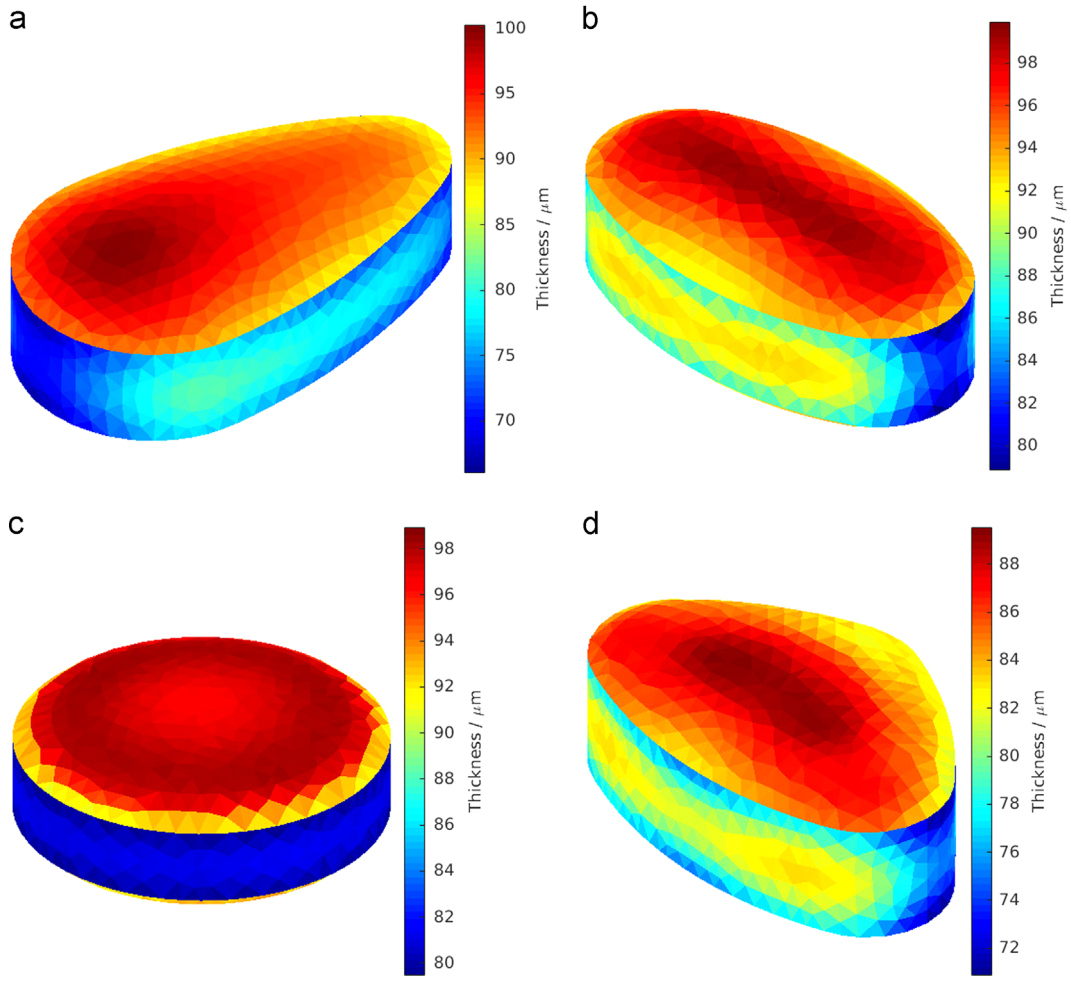

Fig. 7. Coating thickness distributions after 1800 s averaged over all tablets for the (a) almond, (b) oval, (c) round, and (d) triangular tablet shapes. Note that the color scales are different for each tablet shape in order to better highlight the differences in coating thicknesses for a given tablet.

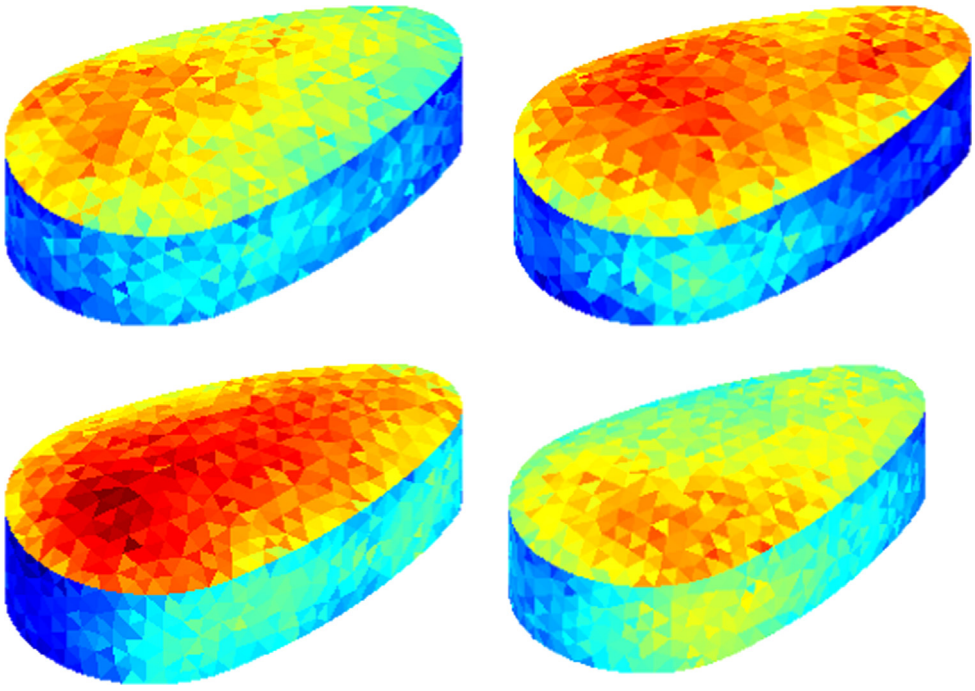

Fig. 8. Predicted coating distributions for four almond tablets chosen randomly in the DEM simulation after 1800 s. The coating mass (actually the number of exposed pixels) for the four tablets is approximately the same.

the DEM-only simulations (Fig. 7). Of particular interest, however, is the comparison of the asymptotic coating thickness maps using the new approach and the approach of Freireich et al. (2011), which does not account for tablet shadowing. Accounting for tablet shadowing, the differences between the cap and band coating thicknesses are smaller and the gradients in coating thickness appear to be less pronounced. These observations are consistent with the smaller asymptotic CoV_{intra} values observed when shadowing is included. This behavior can be expected since the tablet cap surface has a preferential orientation toward the spray. When a tablet is hidden from the spray by tablets in front of it, the amount of coating received by the cap will be smaller and thus the difference in coating thickness between the bands and caps will also be smaller.

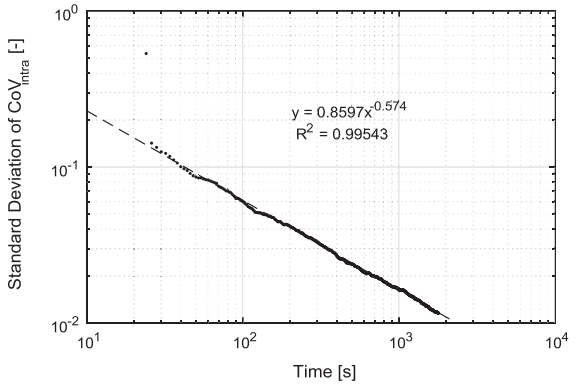

Fig. 9. The standard deviation in individual round tablet CoV_{intra} values plotted as a function of time. Note that the axes are logarithmic. The line in the figure is a power law fit to the data. The data start after all of the tablets have at least some coating on them.

8.3. Comparison of model predictions to experimental measurements

In order to compare the results between DEM and experimental measurements, a scaling factor must be obtained to convert from pixels per unit area to thickness in microns. This scaling factor can be obtained by setting the experimentally measured average film thickness for the entire batch of tablets equal to the average pixels per unit area obtained from DEM. However, making THz measurements over the entire batch of tablets would be extremely time-consuming and only a few tablet samples were measured as listed in Table 5. Note that there is a significant variation in the coating distribution over the tablets as shown in Fig. 8 for four almond tablets selected randomly from the DEM simulation. Thus, the average coating distribution over a few tablet samples may not be representative of the average coating distribution over the entire batch. The largest number of tablets was sampled for the almond shape and the scaling factor was obtained by matching the average film thickness to the average pixels per unit area for the almond tablets. The scaling factor was found to be $k_V = 3 \times 10^{-8}$ μm per pixel per unit area using this approach. Note that debossment features appear in the experimental measurements of the almond and triangular tablet shapes and not in the simulations.

Fig. 13 shows a comparison of the average film thickness distribution over the surface of various tablet shapes. Reasonable agreement is obtained between the experiments and DEM simulations. In particular, the experiments and simulations show that the cap receives more coating compared to the band. The experiments and simulations also show that the small radius of curvature ends of the oval and triangular tablets have smaller coating thicknesses than the larger radius of curvature portions. The effect is less pronounced in the experimental measurements for the almond

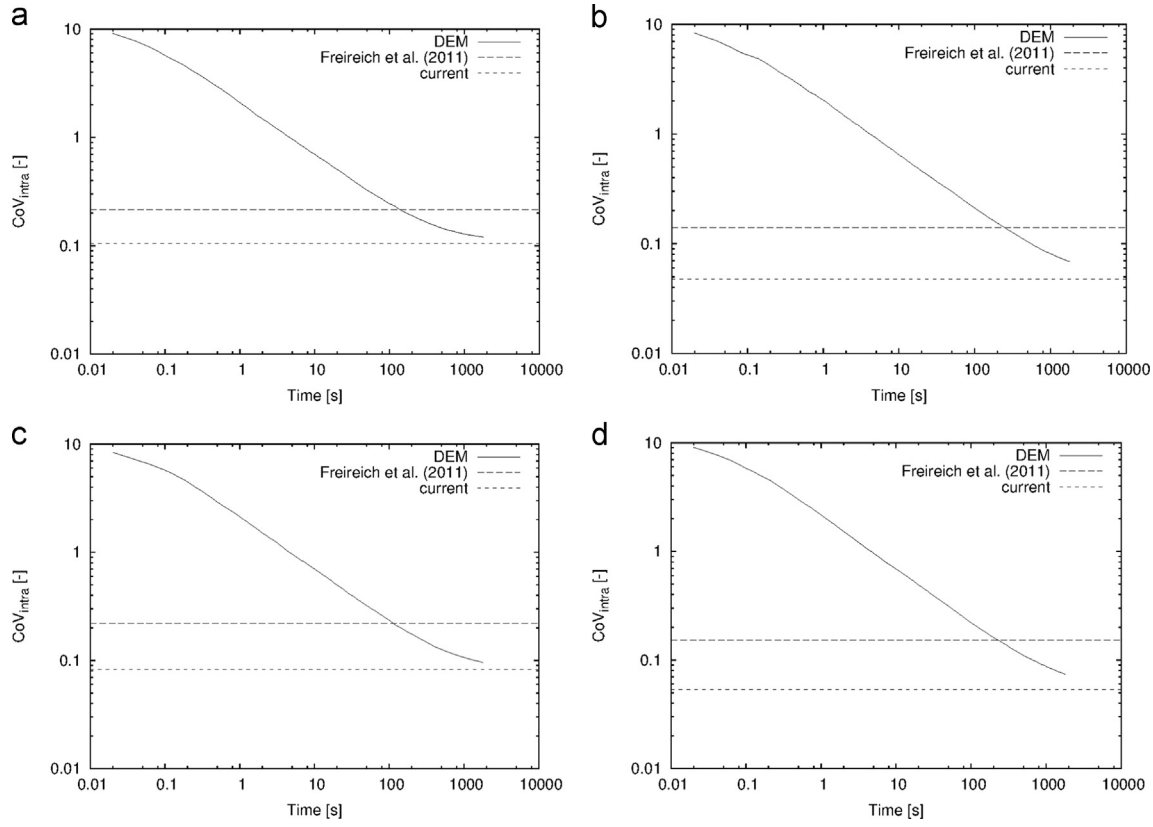

Fig. 10. Predictions of the asymptotic CoV_{intra} values from the multiscale model of Freireich et al. (2011) and the model described in Section 5 superimposed over the data from Fig. 6. (a) Almond, (b) oval, (c) round, and (d) triangular.

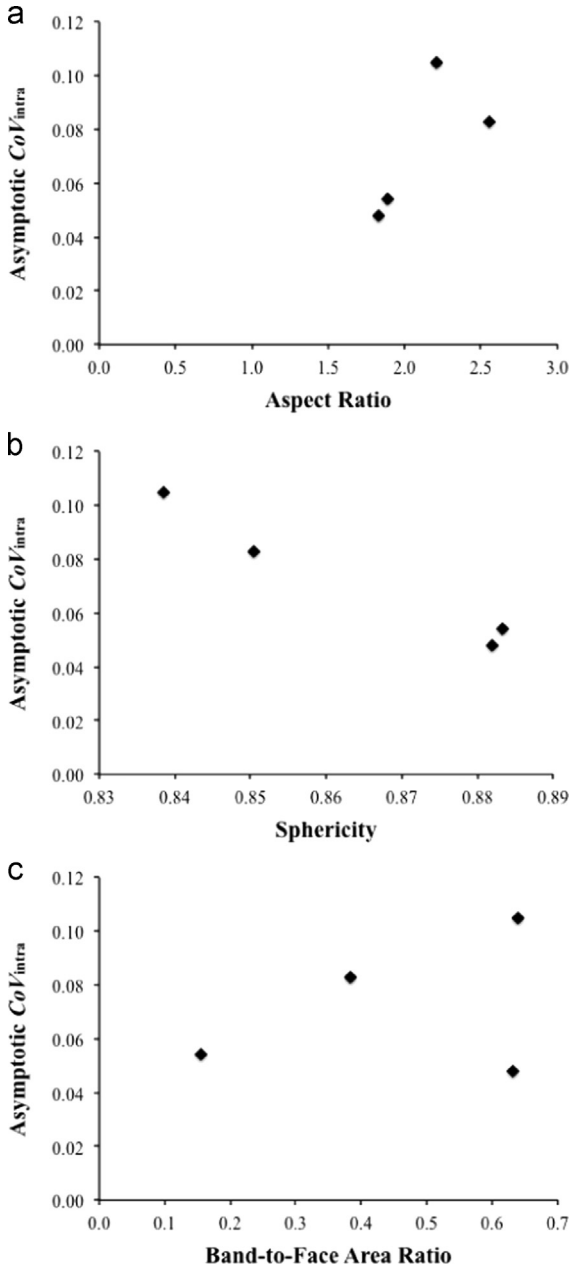

Fig. 11. The asymptotic CoV_{intra} plotted as a function of the tablet (a) aspect ratio, (b) sphericity, and (c) band-to-face surface area ratio.

shape, but it can still be observed. Similarly, the coating thickness is largest near the edges of the cap for the round tablet in both the simulations and experiments. Note that even if a large number of tablets were sampled to provide increased confidence in the experimental coating thickness distributions, the comparisons between experiments and simulations would still be qualitative since different spray patternations and flux distributions were used in the experiments and simulations. Also, these modeling techniques do not account for finite sized drops with finite drying times.

9. Conclusions

Two new modeling approaches for studying intra-tablet coating variability are developed in this work. An image based method, which utilizes a graphics processing unit, tracks the exposure of small area panels on each tablet's surface to a simulated "spray". This method is an extension of a similar approach used for studying inter-tablet coating uniformity (Kumar et al., 2014). The second model is an asymptotic limit model that uses DEM data to coat a "representative tablet". In addition to accounting for tablet orientations, this new model includes the influence of neighboring tablets shadowing a given tablet's exposure to the simulated spray.

Data from the current DEM simulations are the first direct evidence that non-spherical tablets approach an asymptotic CoV_{intra} value. These data support previous analytical work (Freireich and Wassgren, 2010) indicating that if tablets have any preferred orientation while in the spray zone, a non-zero limiting intra-tablet coating uniformity will occur. The asymptotic limits are predicted well from relatively small portions of the DEM data using the new representative tablet asymptotic prediction model. Furthermore, the new model is far more efficient than using a DEM-only approach.

In general, the tablet caps have thicker coatings than the tablet bands, consistent with previous work (e.g., Pérez-Ramos et al., 2005). Moreover, tablets that have a more elongated shape tend to have less coating on the smaller radius of curvature portions of the bands. This behavior is consistent with the idea that the more easily a tablet can roll and expose surfaces to the spray, the more uniformly coated it will be. It is important to note that although randomly selected tablets from the DEM simulations displayed similar coating distributions, the coating distribution on an individual tablet can vary significantly from the coating thickness distribution averaged over all of the tablets. After a sufficiently large period of time, the individual tablet CoV_{intra} values are normally distributed with the standard deviation decreasing with the time in a power law manner. Hence, if intra-tablet coating thickness is a critical parameter, care should be taken to sample a large number of tablets to better estimate the statistics of the population as well as coat for a longer period of time to improve the consistency in CoV_{intra} between tablets.

Of particular importance in this new asymptotic modeling approach is the inclusion of shadowing effects. When shadowing is not included and only tablet orientation is considered, as was done in a previously published model (Freireich et al., 2011), the simulations over-predict the asymptotic CoV_{intra} values and also change the observed rank order of the asymptotic values for different tablet shapes. Hence, tablet shadowing is a significant effect that acts to decrease the asymptotic CoV_{intra}, i.e., improve intra-tablet coating uniformity. Shadowing reduces the amount of coating collected on surfaces that preferentially face the spray and, hence, reduces the coating thickness differences between all of the tablet surfaces.

The asymptotic CoV_{intra} values correlate reasonably well with tablet sphericity, with increasing sphericity improving coating uniformity. This result is in agreement with prior work (Wilson and Crossman, 1997; Ketterhagen, 2011; Freireich et al., 2011). Larger sphericity tablets are expected to roll more easily while passing through the spray zone and thus will have less of a tendency to present the same surfaces to the spray zone with repeated visits through the spray zone.

This paper also presents the first attempt to directly compare experimental and simulated coating thickness distributions. The DEM predictions of coating thickness after 1800 s compare well qualitatively with terahertz thickness measurements made on tablets from coating experiments. Unfortunately only qualitative comparisons could be made due to the limited number of tablets sampled experimentally and differences in exact spray zone areas and flux distributions. The tablets in the experiments, however, displayed similar features as those found in the simulations. In order to produce a larger number of experimental measurements, future work should consider reducing the spatial resolution of coating thickness measurements and/or reduce the dimensions of

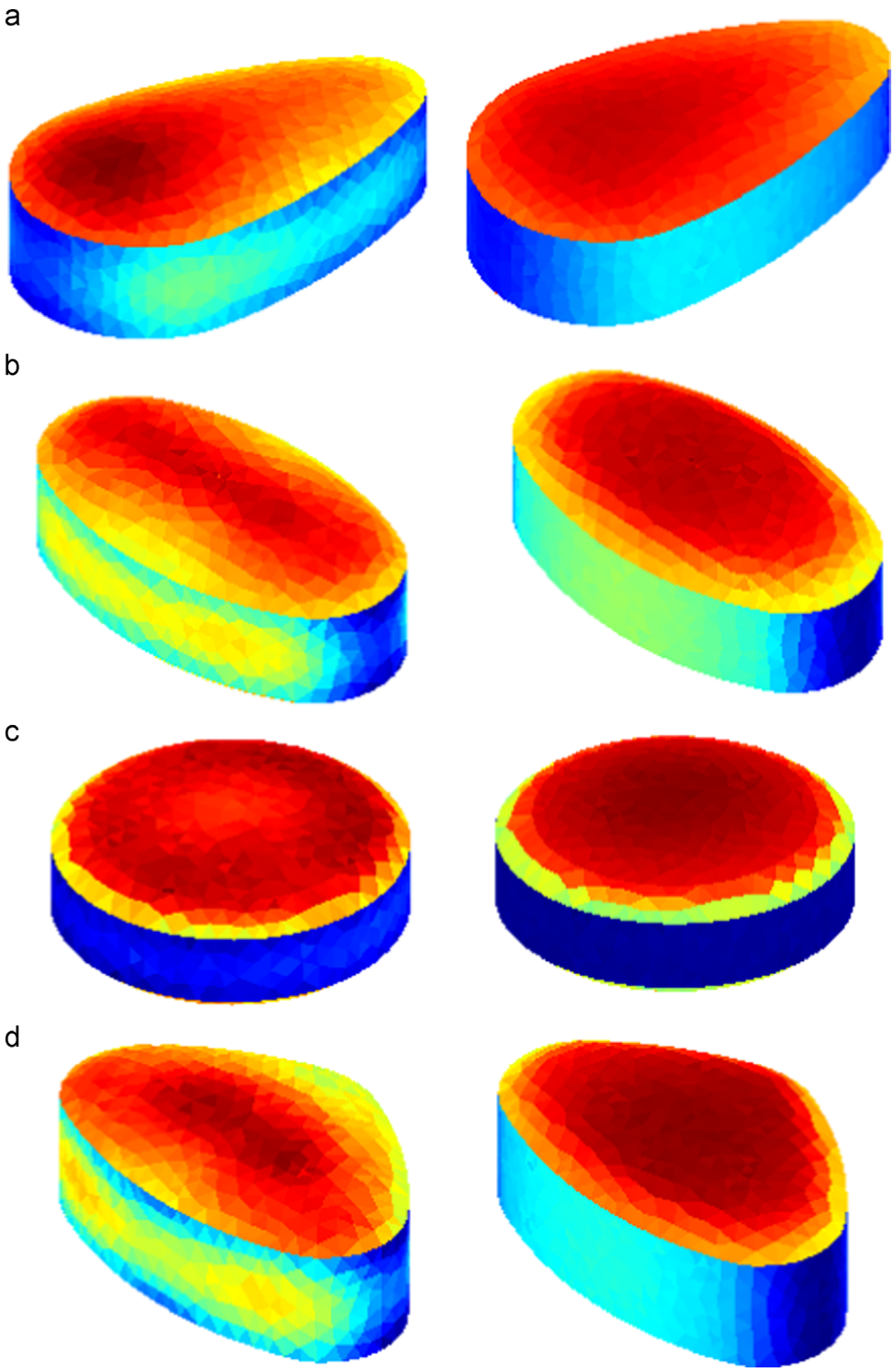

Fig. 12. Asymptotic coating thickness maps generated using (left) the model described in Section 5, and (right) the previous model by Freireich et al. (2011). (a) Almond, (b) oval, (c) round, and (d) triangular. The same color scale is used each left/right tablet pair. (For interpretation of the references to color in this figure legend, the reader is referred to the web version of this article.)

the tablets. The simulations could be used as a guide for which locations are likely to produce the thickest and thinnest coatings for making experimental measurements at reduced spatial resolutions.

The current work demonstrates that intra-tablet coating uniformity is strongly affected by the tablet shape, sphericity in particular, and, at least up to a point, the number of times tablets pass through the coating spray, which increases with increasing pan speed and coating duration, and decreases with fill level. For a sufficiently large number of passes through the spray zone, however, the coefficient of variation in intra-tablet coating thickness will asymptote to a constant value, in contrast to inter-tablet coating variability which continues to decrease with more passes through the spray zone.

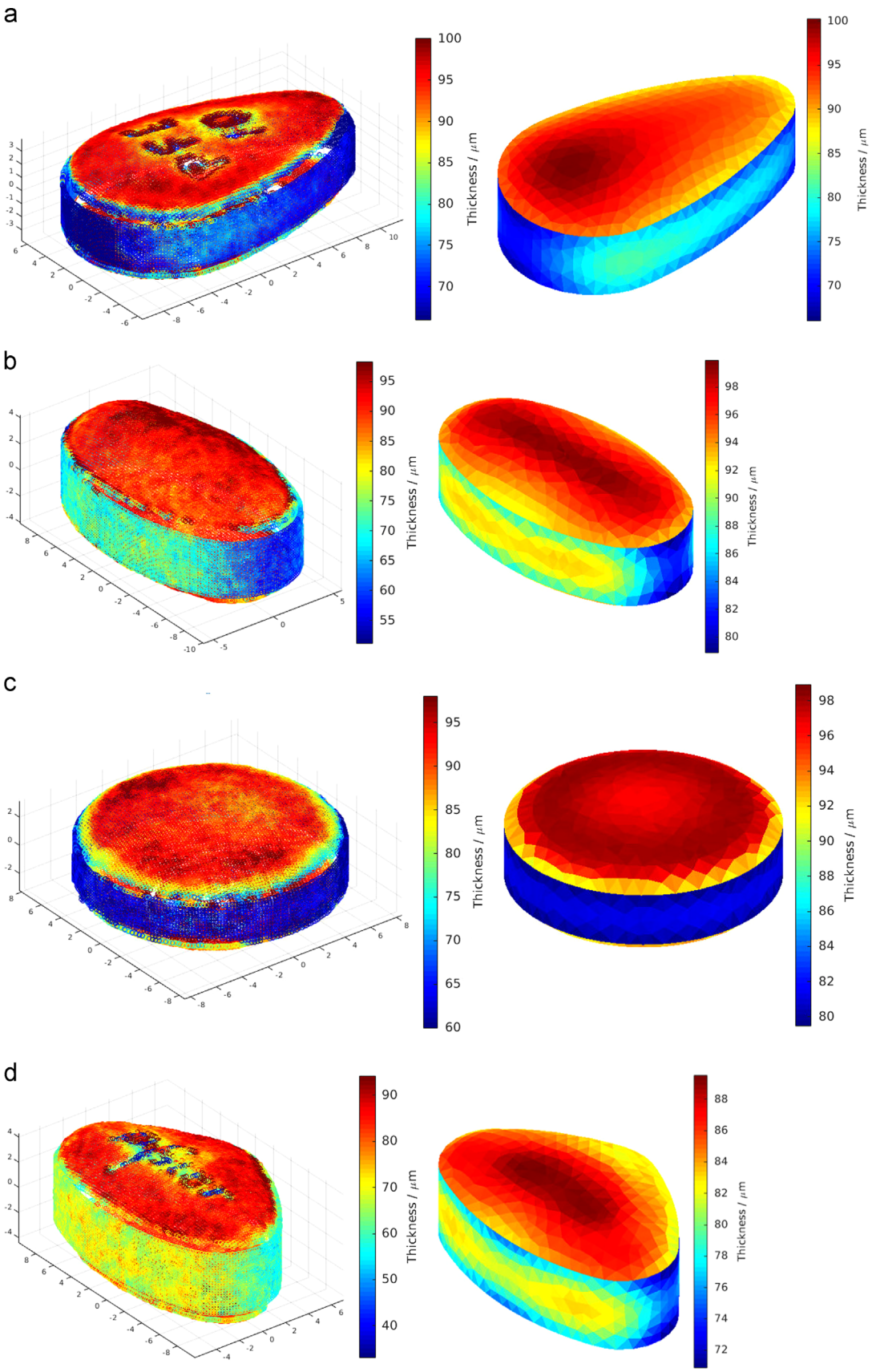

Fig. 13. Coating thickness distributions from the (left) experiments and (right) DEM predictions after 1800 s. (a) Almond, (b) oval, (c) round, and (d) triangular tablet shapes.

Acknowledgments

The authors would like to thank Bob Green from Pfizer for manufacturing the tablets used in this study. R. Kumar and C. Wassgren are grateful to the National Science Foundation Engineering Research Center for Structured Organic Particulate Systems (NSF ERC-SOPS, 0951845-EEC) for financial support. K. Su and J.A. Zeitler would like to acknowledge the UK Engineering and Physical Science Research Council (EP/L019922/1 and EP/K503721/1).

Appendix A. Comparisons of different methods for determining the average CoV_{intra} for a batch of tablets

Several approaches may be used to determine the average CoV_{intra} for a batch of tablets. Four of these methods are described and compared in this Appendix.

A.1 Averaging over each tablet

In this scheme, the coating thickness mean and variance are calculated for each tablet and the bulk CoV_{intra} is found by averaging over all tablet values of CoV_{intra}. The mean thickness for a tablet i, μ_i, is

$$\mu_i = \frac{1}{A}\sum_{j=1}^{N_p} h_{ij}A_j, \tag{9}$$

where N_p is the total number of panels on the tablet, h_{ij} is the thickness on panel j of tablet i, A_j is the area of panel j, and A is the total area of tablet i. The variance in thickness over tablet i is

$$\sigma_i^2 = \frac{1}{A}\sum_{j=1}^{N_p} (h_{ij}-\mu_i)^2 A_j. \tag{10}$$

The corresponding coefficient of variation for tablet i is

$$CoV_{\text{intra},i} = \frac{\sigma_i}{\mu_i}. \tag{11}$$

The average coefficient of variation for the bulk is

$$CoV_{\substack{\text{intra, bulk,}\\ \text{"each tablet"}}} = \frac{1}{N}\sum_{i=1}^{N} CoV_{\text{intra},i}, \tag{12}$$

where N is the total number of tablets. Note that during the early stages of coating, not every tablet may have coating on it and thus the CoV_{intra} for an individual tablet is undefined. Thus, it is most appropriate to use this method of calculating the bulk CoV_{intra} only after a sufficiently large number coating trials so that all tablets have at least some coating.

A.2 Averaging moments

In this scheme, the bulk CoV_{intra} is determined from the ratio of the mean coating thickness and mean variance, which in turn are calculated from the corresponding means for each tablets. This scheme is similar to the method used in Freireich and Wassgren (2010) and Freireich et al. (2011) if the expectation is equated to averaging over the batch of tablets. The mean coating thickness, mean variance, and bulk CoV_{intra} are

$$\mu_m = \frac{1}{N}\sum_{i=1}^{N} \mu_i, \tag{13}$$

$$\sigma_m^2 = \frac{1}{N}\sum_{i=1}^{N} \sigma_i^2, \tag{14}$$

$$CoV_{\substack{\text{intra, bulk,}\\ \text{"average moments"}}} = \frac{\sigma_m}{\mu_m}. \tag{15}$$

A.3 Average tablet

In this scheme, the bulk CoV_{intra} is based on a mean coating thickness and variance calculated using an average thickness distribution found by averaging the thickness distributions over all tablets. The average thickness distribution results in an "average" tablet.

The coating thickness on panel j averaged over all tablets is

$$h_j = \frac{1}{N}\sum_{i=1}^{N} h_{ij}. \tag{16}$$

The mean thickness averaged over this "average" tablet is

$$\mu_t = \frac{1}{A}\sum_{j=1}^{N_p} h_j A_j, \tag{17}$$

and the corresponding variance is

$$\sigma_t^2 = \frac{1}{A}\sum_{j=1}^{N_p} (h_j-\mu_t)^2 A_j. \tag{18}$$

The bulk CoV_{intra} using these values is

$$CoV_{\substack{\text{intra, bulk}\\ \text{"average tablet"}}} = \frac{\sigma_t}{\mu_t}. \tag{19}$$

A.4 Total area

For the "total area" scheme, the mean coating thickness and variance are calculated over all the tablet panels simultaneously

$$\mu_T = \frac{1}{AN}\sum_{i=1}^{N}\sum_{j=1}^{N_p} h_{ij}A_j, \tag{20}$$

$$\sigma_T^2 = \frac{1}{AN}\sum_{i=1}^{N}\sum_{j=1}^{N_p} (h_{ij}-\mu_T)^2 A_j, \tag{21}$$

$$CoV_{\substack{\text{intra, bulk}\\ \text{"total area"}}} = \frac{\sigma_T}{\mu_T}. \tag{22}$$

A.5 Comparing the different schemes

A.5.1 Means

Each method gives the same average coating thickness for the bulk. For example, combining Eqs. (17) and (16) gives

$$\mu_t = \frac{1}{A}\sum_{j=1}^{N_p}\left[\left(\frac{1}{N}\sum_{j=1}^{N} h_{ij}\right)A_j\right]. \tag{23}$$

while combining Eqs. (13) and (9) (i.e., the average of average coating thickness) produces

$$\mu_m = \frac{1}{N}\sum_{i=1}^{N}\left(\frac{1}{A}\sum_{j=1}^{N_p} h_{ij}A_j\right). \tag{24}$$

Switching the order of summation shows that Eqs. (23) and (24) are identical and equal to Eq. (20), i.e.,

$$\mu_t = \mu_m = \mu_T. \tag{25}$$

A.5.2 Variances

Now consider the variances for the "averaging moments" and "total area" approaches. Combining Eqs. (14) and (10) gives the following expression for the "averaging moments" variance:

$$\sigma_m^2 = \frac{1}{N}\sum_{i=1}^{N}\frac{1}{A}\sum_{j=1}^{N_p}(h_{ij}-\mu_i)^2 A_j. \tag{26}$$

The variance for the "total area" approach (Eq. (21)) may be modified by adding and subtracting μ_i,

$$\sigma_T^2 = \frac{1}{AN}\sum_{i=1}^{N}\sum_{j=1}^{N_p}(h_{ij}-\mu_i+\mu_i-\mu)^2 A_j, \tag{27}$$

expanding the squared term

$$\sigma_T^2 = \frac{1}{AN}\sum_{i=1}^{N}\sum_{j=1}^{N_p}\left[(h_{ij}-\mu_i)^2+2(h_{ij}-\mu_i)(\mu_i-\mu)+(\mu_i-\mu)^2\right]A_j, \tag{28}$$

and re-arranging terms

$$\sigma_T^2 = \underbrace{\frac{1}{N}\sum_{i=1}^{N}\overbrace{\frac{1}{A}\sum_{j=1}^{N_p}(h_{ij}-\mu_i)^2 A_j}^{\sigma_i^2}}_{\sigma_m^2} + \underbrace{\frac{1}{N}\sum_{i=1}^{N}(\mu_i-\mu)^2}_{\sigma_{inter}^2}. \tag{29}$$

Eq. (29) may be summarized as

$$\sigma_T^2 = \sigma_m^2 + \sigma_{inter}^2. \tag{30}$$

The first term in Eq. (29) is simply Eq. (26) while the second term represents the variance of average (per tablet) coating thickness between tablets, i.e., the inter-particle coating thickness variance. Therefore, $\sigma_T \geq \sigma_m$, with the equality only holding when there is no inter-tablet variability. Since the means are the same for the two approaches, $CoV_{\text{intra,bulk,"average moments"}} < CoV_{\text{intra,bulk,"total area"}}$.

Now compare the variances using the "average tablet" and the "average moments" approach. Combining Eqs. (18), (16), and (13) along with Eq. (25) gives

$$\sigma_t^2 = \frac{1}{A}\sum_{j=1}^{N_p}\left(\frac{1}{N}\sum_{i=1}^{N}h_{ij}-\frac{1}{N}\sum_{i=1}^{N}\mu_i\right)^2 A_j, \tag{31}$$

or,

$$\sigma_t^2 = \frac{1}{A}\sum_{j=1}^{N_p}\left[\frac{1}{N}\sum_{i=1}^{N}(h_{ij}-\mu_i)\right]^2 A_j. \tag{32}$$

This expression is similar to Eq. (26), but here the entire internal sum is squared rather than just the summand. The squared sum must satisfy the Cauchy–Schwartz inequality

$$\left[\frac{1}{N}\sum_{i=1}^{N}(h_{ij}-\mu_i)\right]^2 \leq \frac{1}{N}\sum_{i=1}^{N}(h_{ij}-\mu_i)^2. \tag{33}$$

Because the right hand side of Eq. (33) must be positive, it follows from Eq. (32)

$$\sigma_t^2 \leq \frac{1}{A}\sum_{j=1}^{N_p}\frac{1}{N}\sum_{i=1}^{N}(h_{ij}-\mu_i)^2 A_j = \sigma_m^2. \tag{34}$$

Therefore, it can be concluded that $CoV_{\text{intra,bulk,"average tablet"}} \leq CoV_{\text{intra,bulk,"average moments"}} < CoV_{\text{intra,bulk,"total area"}}$, where the last inequality comes from the "average moments" and "total area" analysis presented previously.

A.6 Comparisons to simulation

In order to better elucidate the differences in averaging schemes, a Monte Carlo simulation of an imaginary coating process is performed. In this simulation, there are N tablets, each with N_p panels. The probability of panel j receiving coating during a given coating trial is p_j. Since the purpose of this simulation is to explore differences in the CoV_{intra} averaging schemes, each of the N_p panels is given a different, arbitrary coating probability. In these Monte Carlo simulations, $p_j=(j/N_p)/10$, which means that 10% of a tablet's surface gets coated during each trial, but each panel has a different probability of being coated. In order to include the effects of inter-tablet coating variability, it is assumed that only a fraction of tablets, $\alpha=0.1$, are coated during each coating trial. The Monte Carlo model generates an array of coating thickness h_{ij} for each coating trial. The simulation is performed for $N=1000$ and $N_p=100$ for 10,000 coating trials. The bulk CoV_{intra} values calculated using the various schemes are shown in Fig. A1.

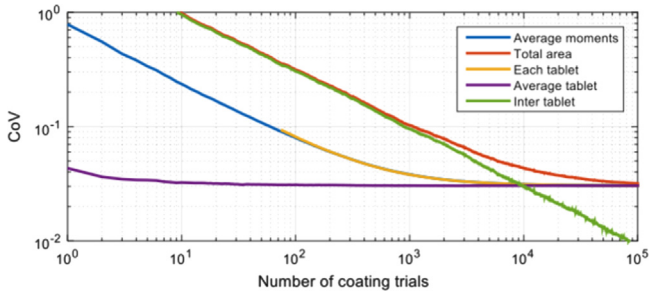

Fig. A1. Bulk CoV_{intra} plotted as a function of the number of coating trials for the various averaging schemes investigated. A Monte Carlo algorithm is used to generate the data.

$CoV_{\text{intra,bulk,"each tablet"}}$ does not exist for a small number of coating trials since not every tablet has coating during this early time. If C is the number of coating trials, the expected fraction of uncoated particles after C coating trials is $1-(1-\alpha)^C$. Therefore, we expect $CoV_{\text{intra,bulk,"each tablet"}}$ to be meaningful when $C > \ln(1.0–0.95)/\ln(1.0–0.9) \approx 30$. The simulation is consistent with this calculation. Interestingly, $CoV_{\text{intra,bulk,"average moments"}}$ and $CoV_{\text{intra,bulk,"each tablet"}}$ are nearly identical for all times that $CoV_{\text{intra,bulk,"each tablet"}}$ exists. This fact is convenient since the analytical methods of Freireich and Wassgren (2010) use $CoV_{\text{intra,bulk,"average moments"}}$, but $CoV_{\text{intra,bulk,"each tablet"}}$ is statistically easier to compare to experimental results. The simulation also shows that $CoV_{\text{intra,bulk,"total area"}}$ is dominated by the inter-tablet variability, which makes its use as a measure of intra-tablet coating variability ineffective. The simulation results are also consistent with the previous analysis showing that $CoV_{\text{intra,bulk,"average tablet"}} \leq CoV_{\text{intra,bulk,"average moments"}} < CoV_{\text{intra,bulk,"total area"}}$. Because CoV_{intra} decreases monotonically towards an asymptotic value, it can therefore be expected that the average tablet scheme should approach the asymptotic limit before the other schemes.

Finally, and most significantly, $CoV_{\text{intra,bulk,"average tablet"}}$ is observed to asymptote within approximately 100 times fewer coating trials than either $CoV_{\text{intra,bulk,"average moments"}}$ or $CoV_{\text{intra,bulk,"each tablet"}}$. In fact, the "average tablet" approach asymptotes at approximately the same number of coating trials as the "each tablet" first exists. The new asymptotic coating trial described in Section 5 uses the "average tablet" approach while the Freireich and Wassgren (2010) work uses the "average moments" approach. Although both averaging schemes give the same asymptotic $CoV_{\text{intra,bulk}}$ value, the "average tablet" approach converges much more quickly. The inter-tablet coating variability decreases with the square root of the number of coating trials, as expected. The small amount of observed noise decreases if N is increases.

References

ANSYS, 2014. ANSYS ICEM CFD, ⟨http://www.ansys.com/Products/Other+Products/ANSYS+ICEM+CFD⟩ (accessed 24.09.14).

Alexander, A., Shinbrot, T., Muzzio, F.J., 2002. Scaling surface velocities in rotating cylinders as a function of vessel radius, rotation rate, and particle size. Powder Technol. 126, 174–190.

Bharadwaj, R., Smith, C., Hancock, B.C., 2010. The coefficient of restitution of some pharmaceutical tablets/compacts. Int. J. Pharm. 402 (1–2), 50–56.

Brock, D., Zeitler, J.A., Funke, A., Knop, K., Kleinebudde, P., 2013. Evaluation of critical process parameters for intra-tablet coating uniformity using terahertz pulsed imaging. Eur. J. Pharm. Biopharm. 85, 1122–1129.

Freireich, B., Litster, J., Wassgren, C., 2009. Using the discrete element method to predict collision-scale behavior: a sensitivity analysis. Chem. Eng. Sci. 64 (15), 3407–3416.

Freireich, B., Wassgren, C., 2010. Intra-particle coating variability: analysis and Monte-Carlo simulations. Chem. Eng. Sci. 65, 1117–1124.

Freireich, B., Ketterhagen, W.R., Wassgren, C., 2011. Intra-tablet coating variability for several pharmaceutical tablet shapes. Chem. Eng. Sci. 66, 2535–2544.

Hancock, B.C., Mojica St, N., John-Green, K., Elliott, J.A., Bharadwaj, R., 2010. An investigation into the kinetic (sliding) friction of some tablets and capsules. Int. J. Pharm. 384 (1–2), 39–45.

Ho, L, Müller, R., Römer, M., Gordon, K.C., Heinämäki, J., Kleinebudde, P., Pepper, M., Rades, T., Shen, Y.C., Strachan, C.J., Taday, P.F., Zeitler, J.A., 2007. Analysis of sustained-release tablet film coats using terahertz pulsed imaging. J. Controlled Release 119, 253–261.

Just, S., Toschkoff, G., Funke, A., Djuric, D., Scharrer, G., Khinast, J., Knop, K., Kleinebudde, P., 2013. Experimental analysis of tablet properties for discrete element modeling of an active coating process. AAPS PharmSciTech 14 (1), 402–411.

Kalbag, A., Wassgren, C., Penumetcha, S.S., Perez-Ramos, J.D., 2008. "Inter-tablet coating variability: Residence times in a horizontal pan coater". Chemical Engineering Science 63 (11), 2881–2894.

Ketterhagen, W.R., 2011. Modeling the motion and orientation of various pharmaceutical tablet shapes in a film coating pan using DEM. Int. J. Pharm. 409, 137–149.

Kumar, R., Freireich, B., Wassgren, C., 2014. DEM-compartment-population balance model for particle coating in a horizontal rotating drum. Chem. Eng. Sci. 125, 144–157. http://dx.doi.org/10.1016/j.ces.2014.06.046.

Madamba, M.C., Mullett, W.M., Debnath, S., Kwong, E., 2007. Characterization of tablet film coatings using a laser-induced breakdown spectroscopic technique. AAPS PharmSciTech 8 (4), E1–E7, Article 103.

Möltgen, C.V., Puchert, T., Menezes, J.C., Lochmann, D., Reich, G., 2012. A novel in-line NIR spectroscopy application for the monitoring of tablet film coating in an industrial scale process. Talanta 92, 26–37.

Pandey, P., Song, Y., Kayihan, F., Turton, R., 2006. Simulation of particle movement in a pan coating device using discrete element modeling and its comparison with video-imaging experiments. Powder Technol. 161, 79–88.

Pérez-Ramos, J.D., Findlay, W.P., Peck, G., Morris, K.R., 2005. Quantitative analysis of film coating in a pan coater based on in-line sensor measurements. AAPS PhatmSciTech 6 (1), E127–E136, Article 20.

Pérez-Ramos, J.D., 2006. Monitoring and Modeling of Film Coating in a Side Vented Pan Coater Using Near-Infrared Reflectance Spectroscopy, Digital Video Imaging and Computational Methods. Purdue University, West Lafayette, IN, U.S.A, Ph.D. thesis.

Russe, I.-S., Brock, D., Knop, K., Kleinebudde, P., Zeitler, J.A., 2012. Validation of terahertz coating thickness measurements using x-ray microtomography. Mol. Pharm. 9, 3551–3559.

Shen, Y., Taday, P.F., 2008. Development and application of terahertz pulsed imaging for nondestructive inspection of pharmaceutical tablet. IEEE J. Sel. Top. Quantum Electron. 14, 407–415.

Suzzi, D., Toschkoff, G., Radl, S., Machold, D., Fraser, S.D., Glasser, B.J., Khinast, J.G., 2012. DEM simulation of continuous tablet coating: effects of tablet shape and fill level on inter-tablet coating variability. Chem. Eng. Sci. 69, 107–121.

Tousey, M.D., 2005. Tablet coating basics. Tablets Capsul. 3 (3), 20–24.

Turton, R., 2008. Challenges in the modeling and prediction of coating of pharmaceutical dosage forms. Powder Technol. 181, 186–194.

Wilson, K.E., Crossman, E., 1997. The influence of tablet shape and pan speed on intra-tablet film coating uniformity. Drug Dev. Ind. Pharm. 23 (12), 1239–1243.

Yamane, K., Nakagawa, M., Altobelli, S.A., Tanaka, T., Tsuji, Y., 1998. Steady particulate flows in a horizontal rotating cylinder. Phys. Fluids 10 (6), 1419–1427.

Zeitler, J.A., Shen, Y., Baker, C., Taday, P.F., Pepper, M., Rades, T., 2007. Analysis of coating structures and interfaces in solid oral dosage forms by three dimensional terahertz pulsed imaging. J. Pharm. Sci. 96, 330–340.